HOKKAIDO UNIVERSITY

Title	The liquid-phase hydrogenation of 1-heptyne over Pd-Au/TiO2 catalysts prepared by the combination of incipient wetness impregnation and deposition-precipitation
Author(s)	Kittisakmontree, Prathan; Pongthawornsakun, Boontida; Yoshida, Hiroshi et al.
Citation	Journal of Catalysis, 297, 155-164 https://doi.org/10.1016/j.jcat.2012.10.007
Issue Date	2013-01
Doc URL	https://hdl.handle.net/2115/52085
Type	journal article
File Information	joc297_155-164.pdf

Hokkaido University Collection of Scholarly and Academic Papers : HUSCAP

The liquid-phase hydrogenation of 1-heptyne over Pd-Au/TiO_2 catalysts prepared by the combination of incipient wetness impregnation and deposition-precipitation

Prathan Kittisakmontree[a], *Boontida Pongthawornsakun*[a], *Hiroshi Yoshida*[b], *Shin-ichiro Fujita*[b], *Masahiko Arai*[b], *and Joongjai Panpranot*[a,*]

[a]Center of Excellence on Catalysis and Catalytic Reaction Engineering, Department of Chemical Engineering, Faculty of Engineering, Chulalongkorn University, Bangkok 10330, Thailand

[b]Division of Chemical Process Engineering, Faculty of Engineering, Hokkaido University, Sapporo 060-8628, Japan

Date: October 4, 2012

Submitted to: *Journal of Catalysis*

[*]To whom all correspondence should be addressed.

Tel.: 66-2218-6869 Fax: 66-2218-6877 E-mail: joongjai.p@chula.ac.th

Abstract

TiO_2 supported Pd-Au catalysts were prepared with Pd (0.5 wt-%) by impregnation and then Au (1.0 wt-%) by deposition – precipitation ($Au/Pd/TiO_2$) and vice versa ($Pd/Au/TiO_2$). For the former sample, the state of dispersion of Pd on TiO_2 changed during the loading of Au, resulting in the formation of small Au – Pd alloy particles and thus changing the electronic properties of Pd species. The alloy formation was not clearly detected on the $Pd/Au/TiO_2$ and the electronic properties of Pd were not so different from those of monometallic Pd/TiO_2. All the catalysts were selective to 1-heptene (> 95%) until close to the complete conversion of 1-hetyne. However, the selectivity of 1-heptene drastically decreased to 0% (which was further hydrogenated to heptane) in 120 min for the $Au/Pd/TiO_2$ while it still remained > 60% for the $Pd/Au/TiO_2$ similar to the monometallic Pd/TiO_2 catalyst. The rate of 1-heptene hydrogenation (in the second step) did not depend on the Pd dispersion but was found to be greatly enhanced as the Pd species became electron-rich in the Au – Pd alloy particles. The modification of Pd species by Au was less significant for the first step of hydrogenation of 1-heptyne to 1-heptene.

Keywords: 1-heptyne, selective hydrogenation, liquid-phase hydrogenation, Pd-Au bimetallic catalysts

1. Introducttion

The reactions involving alkyne and alkene hydrogenation have become of both industrial and academic importance. A number of products from these reactions are used in the food (flavors), pharmaceutical (sedatives, anesthetics, vitamins), cosmetics (fragrances), plastics (resins and polymers), and lubricants industries [1]. Such reactions are often carried out in three-phase catalytic systems using batch and semibatch reactors. Different alkynic compounds have been employed as model reactants for evaluation of the liquid-phase selective hydrogenation catalysts under mild reaction conditions such as 1-hexyne [2-3], 3-hexyne [4], 1-heptyne [1,5-7], 4-octyne [8], phenylacetylene [9,10], and 1-phenyl-1-pentyne [11]. Palladium is the most common hydrogenation catalyst used in industry and studied in fundamental research because of its ability to selectively hydrogenate multiple unsaturated hydrocarbons.

The promotional effect of Au in Pd–Au catalysts has been well established in many catalytic processes. The well-known applications include CO oxidation, selective oxidation of alcohols to aldehydes or ketones, alkenes to epoxides, and oxidation of hydrogen to hydrogen peroxide [12-15]. Superior activities of Au–Pd catalysts, as compared to the monometallic Pd or Au nanoparticles, have been attributed to the synergistic effects arisen from both ligand effects and ensemble effects of the Au-Pd alloy [16]. Despite the low reactivity of Au in hydrogenation, Au and Pd–Au catalysts have been studied in the selective hydrogenation of various compounds such as aromatic compounds [17-19], acetylene [19,20], 1,3-butadiene [21], 1,3-cyclooctadiene [22], cinnamaldehyde [23], and citral [24]. Different roles of Au addition have been reported in the selective hydrogenation over support Pd catalysts. Deposition of Au particles was used for selective poisoning of Pd surface in the selective hydrogenation of acetylene [20]. In the benzaldehyde hydrogenation in the presence of sulfur, gold

acted as only an inert diluent that prevented Pd_4S formation without changing the catalyst activity [25]. A number of studies show that electron transfer between Pd and Au species occurred and was responsible for the improvement in both catalytic activity and selectivity in the hydrogenation reactions [17,23,24].

The majority of previous reports in the alkyne hydrogenation over Pd–Au bimetallic catalysts focused on the gas-phase selective hydrogenation of low molecular weight substrates, mostly acetylene. The liquid-phase hydrogenation of higher molecular weight alkynes on Pd–Au catalysts is scarcely reported. Parvulescu et al. [26] showed that enhanced activity and improved selectivity were obtained over the colloidal Pd-Au particles embedded in silica sol-gel matrix with 0.6 and 1 wt % metal loading in the liquid-phase selective hydrogenation of 3-hexyn-1-ol. Scott et al. [27] reported the catalytic activity of bimetallic Pd–Au nanoparticles solubilized in 1-butyl-3-methylimidazolium hexafluorophosphate ionic liquid with poly(vinylpyrrolidone) as a stabilizer in the liquid-phase hydrogenation of 1,3-cyclooctadiene, cinnamaldehyde, and 3-hexyn-1-ol. The activity and selectivity of the hydrogenation reactions were varied depending on the Au–Pd composition. Supported Pd–Au catalysts prepared by non-colloidal routes were seldom studied in the liquid-phase alkyne hydrogenation.

In the present work, TiO_2 supported Pd-Au catalysts were prepared by the combination of incipient wetness impregnation (IM) and deposition-precipitation (DP) methods. Such methods are among the most commonly used methods for the preparation of supported monometallic Pd and Au catalysts, respectively. The catalysts were prepared with either loading of Au (1 wt%) first by DP method followed by IM of Pd (0.5 wt%) or preparation of Pd/TiO_2 first by IM before loading of Au by DP. Loading sequence was found to strongly affect the characteristics and catalytic behavior of the bimetallic $Pd–Au/TiO_2$ catalysts prepared in the liquid-phase

hydrogenation of 1-heptyne. The catalytic performances were correlated with the catalyst characterization results obtained from various techniques such as X-ray diffraction (XRD), transmission electron microscopy (TEM), CO chemisorption, X-ray photoelectron spectroscopy (XPS), and UV-Vis spectroscopy.

2. Experimental

2.1 Catalyst preparation

The TiO_2 support was pure anatase titanium dioxide obtained commercially from Fluka. It has the specific surface area 10 m^2/g, pore volume 0.02 cm^3/g, and average pore diameter 7.6 nm. Loading of Pd (ca. 0.5 wt%) was done by the IM technique using 1 M HCl solution of $PdCl_2$ (99.999% Aldrich). The catalysts were dried overnight at 110^{o}C and calcined in air at 500^{o}C for 2 h. Deposition of Au nanaparticles (ca. 1 wt%) was carried out by the DP method according to the method described in Ref.[28]. Firstly, $HAuCl_4.3H_2O$ (99.9+% metal basis, Aldrich) was dissolved in 100 cm^3 deionized water. The pH was adjusted to 7 by using 0.1 M of NaOH. The TiO_2 support or the Pd/TiO_2 catalyst was dispersed in the solution and the pH was adjusted again to 7 with 0.1 M NaOH. The suspension was vigorously stirred for 2 h at 80^{o}C. After that the suspension was cooled and centrifuged five times with deionized water in order to remove chloride and then dried at 110^{o}C. The catalyst nomenclatures according to the different metal loading sequences are shown in **Table 1**.

2.2 Catalyst characterization

The XRD patterns of the catalysts prepared were measured from 10 to 80^o 2θ using a SIEMENS D5000 X-ray diffractometer and Cu K_α radiation with a Ni filter. TEM was carried out using a JEOL JEM 2010 transmission electron microscope that

employed a LaB_6 electron gun in the voltage range of 80–200 kV with an optical point to point resolution of 0.23 nm. The XPS measurement was carried out using an AMICUS photoelectron spectrometer equipped with an Mg K_α X-ray as a primary excitation and KRATOS VISION2 software. XPS elemental spectra were acquired with 0.1 eV energy step at a pass energy of 75 eV. All the binding energies were referenced to the C 1s peak at 285.0 eV of the surface adventitious carbon. The UV-Vis diffuse reflectance spectra (DSR) were recorded using a Shimadzu UV-3100PC spectrophotometer from 200 to 800 nm. The relative percentages of palladium dispersion were determined by CO pulse chemisorption at 40^{o}C using a BEL-METAL-1 system. Approximately 0.1 g of catalyst was reduced under hydrogen flow at 40^{o}C for 2 h, and then helium was purged. The CO was pulsed over the reduced catalyst until the TCD signal from the pulse was constant.

2.3 Reaction study in the liquid-phase hydrogenation of 1-heptyne

The liquid-phase hydrogenation of 1-heptyne (98%, Aldrich) was carried out in a magnetically stirred 50-cm^3 teflon-lined stainless steel autoclave reactor. Prior to the reaction testing, the catalyst sample was reduced by hydrogen gas at a flow rate of 50 cm^3/min at 40^{o}C for 2 h. Then, 0.01 g of the sample was dispersed in 10 cm^3 of toluene (99.9%, Merck) containing 2 vol.% 1-heptyne. The effect of mass transfer on the reaction rate was negligible by using a high stirring rate (1000 rpm). The reaction was carried out under flowing hydrogen at 1 bar and 30^{o}C for 10-120 min. The liquid reactants and products were analyzed by a gas chromatograph equipped with an FID detector (Shimadzu GC-14A and TC-WAX column).

3. Results and discussion

3.1 Catalyst characterization

3.1.1 XRD and TEM

The XRD patterns of the TiO_2 support and supported catalysts are shown in **Figure 1**. The characteristic peaks of pure anatase phase titania were observed $2\theta = 25^o$ (major), 37^o, 48^o, 55^o, 56^o, 62^o, 71^o, and 75^o [29] without contamination of other phases such as rutile and brookite for all the samples. The XRD characteristic peaks corresponding to palladium and gold species were not detected for the Au/TiO_2, Pd/TiO_2, and $Au/Pd/TiO_2$ because of the low amount of metals present and, probably, the very high intensity of the TiO_2 peaks (due to the large TiO_2 crystallite size ~100 nm) compared to the crystallite size of the metals. For the $Pd/Au/TiO_2$, additional peaks at $2\theta = 38^o$ and 44^o were observed and were indexed to cubic gold metal [30]. The appearance of these Au metallic peaks in the XRD pattern indicated that the Au particles were fairly large in this sample (comparable to the TiO_2).

Typical TEM images and particle size distributions of the monometallic Au/TiO_2 and Pd/TiO_2 are shown in **Figure 2**. The TiO_2 support had a uniform particle size of 0.1-0.2 μm. The metal dispersion of the catalysts can be seen from the TEM images. The average particle sizes of the Au/TiO_2 and Pd/TiO_2 catalysts were 10.3 and 6.9 nm, respectively. The particle size of Au was larger than expected because it was previously reported that 2-3 nm Au nanoparticles were formed on the P25-TiO_2 by a similar method as used in this work [28]. The formation of larger Au particles may be attributed to the lower surface area of the TiO_2 support used in this study (~10 m^2/g). An adequate support seems to be necessary for preparation of well-dispersed monometallic gold nanoparticles with high activity [31]. In general, gold particles prepared by DP are associated with small particle sizes with a uniform particle size distribution [32] and a closed interaction between the gold particles and the support

[33]. The smaller size of Pd particles indicates a better dispersion of palladium on this TiO_2 support.

The TEM images of the bimetallic $Pd/Au/TiO_2$ and $Au/Pd/TiO_2$ are shown in **Figure 3** and **4**, respectively. For the $Pd/Au/TiO_2$ catalyst, in which Au was loaded on the TiO_2 by DP in the first step followed by IM Pd in the second step, large particles being 30-50 nm in size was observed in addition to some 2-8 nm particles. The larger particles can be attributed to Au^0 particles according to the XRD results. However, further characterization by XPS and UV-Vis spectroscopy (discussed hereafter) suggests the coverage of Au surface by Pd. The formation of Pd–Au alloy particles with relatively large size (i.e. > 30 nm) has often been reported for supported Pd–Au catalysts prepared by co-impregnation of $PdCl_2$ and $HAuCl_4$ [34,35]. In the present study, Au particles on the Au/TiO_2 may be unstable during the IM of HCl solution containing $PdCl_2$ and hydrolyzed to form $AuCl_4$ or $Au(OH)Cl_3$ gold species. Under acidic pH, these gold species interacted repulsively with the positively charged TiO_2 surface, resulting in the growth of Au precipitated [36-37]. The subsequent calcination then resulted in the formation of PdO on both large Au aggregates and the TiO_2 support. For the $Au/Pd/TiO_2$ catalyst, in which the Au nanoparticles were deposited on the Pd/TiO_2 by DP in the second step after IM and calcination of Pd, higher metal dispersion was seen from the TEM images (Figure 4). The sample shows a bimodal particle size distribution of average sizes 1.7 and 7.9 nm.

3.1.2 XPS

The surface properties and the chemical states of Pd and Au on the different catalysts were investigated by XPS. Prior to the measurements, all the catalysts were reduced *ex-situ* in H_2 flow at 40^{o}C for 2 h and kept in a dessicator. The Pd 3d spectra

of the catalysts are shown in **Figure 5**. For the Pd/TiO_2 and $Pd/Au/TiO_2$, the binding energy of Pd $3d_{5/2}$ were detected at 336.5-336.8 eV and were attributed to the presence of palladium in the form of PdO [38]. The binding energy of Pd 3d in the $Pd/Au/TiO_2$ and Pd/TiO_2 were essentially similar, suggesting that electronic structure of the surface Pd atoms was not changed in the presence of large Au particles in the case of $Pd/Au/TiO_2$. The presence of PdO on the surface was ascribed to the easy oxidation of Pd upon contact with air at room temperature. Herzing et al. [34] reported that some surface oxide layer of PdO persisted even after the reduction treatment.

On the other hand, the Pd 3d spectra of the $Au/Pd/TiO_2$ catalyst were fitted by two peaks at higher and lower binding energies of 336.2 eV and 335.2 eV, which were attributed to Pd–Au alloy and metallic Pd^0, respectively [39,40]. In addition, these Pd particles were highly resistant to oxidation, compared to those of the Pd/TiO_2 and $Pd/Au/TiO_2$. Previous studies by Qian and Huang [41] and Yang et al. [42] confirmed that adding Au was helpful to the reduction of Pd^{2+} to metallic Pd, or the protection of Pd^0 from being oxidized into PdO. The atomic percent of the species at 336.2 eV and 335.2 eV were determined by peak fitting to be 15% and 85%, respectively.

The XPS core level spectra of Au 4f of the various catalysts are shown in **Figure 6**. The Au 4f peaks were detected at a range of binding energy (B. E.) of 83.0-83.1 eV for the Au/TiO_2 and $Au/Pd/TiO_2$ catalysts, which is typical of metallic gold (B.E. 84.0 ± 0.1) [41]. The Au 4f peaks were not obviously seen for the $Pd/Au/TiO_2$ catalyst. The atomic concentrations of Pd and Au determined by XPS are given in **Table 2**. The percentage of Pd on the surface was found to increase in the order: $Au/Pd/TiO_2 > Pd/Au/TiO_2 > Pd/TiO_2$ whereas that of Au is shown as $Au/Pd/TiO_2 > Au/TiO_2 > Pd/Au/TiO_2$. The XPS results suggest the coverage of Au surface by Pd for

the Pd/Au/TiO_2. In contrast, Pd–Au alloy particles with Au-rich on the surface may be formed on the Au/Pd/TiO_2.

3.1.3 CO pulse chemisorption and UV-Vis

The CO chemisorption results are given in **Table 2**. The dispersion of Pd increased in the order: Au/Pd/TiO_2 > Pd/TiO_2 > Pd/Au/TiO_2. The calculated Pd^0 particle size of the Pd/TiO_2 was in good agreement with that observed by TEM. For the bimetallic Pd/Au/TiO_2 and Au/Pd/TiO_2, the calculated Pd^0 particle sizes were larger and smaller than the monometallic Pd/TiO_2, respectively. For the Pd/Au/TiO_2, the presence of large Au aggregates probably lower the dispersion of Pd on the TiO_2 due to limited surface area of the support and some PdO species may form on the Au particles. On the contrary, the higher dispersion of Pd on the Au/Pd/TiO_2 was ascribed to the restructuring/redispersion of Pd particles during DP of Au particles.

The UV/Vis spectra of the mono and bimetallic catalysts are shown in **Figure 7**. The Au/TiO_2 exhibited the typical Au plasmon band at 570 nm [43]. The dampening and broadening of the Au plasmon band for the Au/Pd/TiO_2 corresponded to the Pd–Au alloy formation [44-46]. The Pd/TiO_2 and Pd/Au/TiO_2 did not show any well-resolved surface plasmon band, which is typical for the monometallic Pd catalysts [30]. The surface of Au particles may be covered by Pd in the Pd/Au/TiO_2, resulting in the disappearance of Au plasmon band. The UV-Vis spectra also suggested that most of the Au particles existed in the Pd–Au alloy and that there was no separate formation of pure Au nanoparticles in the bimetallic catalyst systems.

3.1.4 Structural features

Figure 8 illustrates the morphology of the different catalysts based on the characterization results. The monometallic Pd/TiO_2 and Au/TiO_2 contained small metal particles with average particle sizes of ca. 6 and 10 nm, respectively. However, these Pd and Au particles were not so stable upon the addition of another metal in the second step. Impregnation of Pd on the Au/TiO_2 led to the formation of large Au particles (~30-50 nm). The aggregation of Au occurred during the drying and calcination steps after the incipient impregnation of HCl solution containing $PdCl_2$. The XPS results showed only Pd species in the form of PdO on the surface at similar binding energies to those of the monometallic Pd/TiO_2, suggesting no alloying in the $Pd/Au/TiO_2$ catalyst. However, the dispersion of Pd was lower in the presence of large Au aggregates and some of the Pd particles may be located on the Au surface.

Addition of Au by DP on the Pd/TiO_2 also changed the state of dispersion of Pd species on TiO_2, but in an opposite trend to that of the $Pd/Au/TiO_2$. The dispersion of Pd increased upon the addition of Au and small Au–Pd alloy particles were formed. The XPS results also suggest the modification of the electronic properties of Pd and the formation of the Pd–Au alloy particles. In fact, the redispersion/restructuring of Pd particles occurred during DP even in the absence of Au precursor. **Figure 9** shows TEM image and particle size distribution of the calcined Pd/TiO_2 after being treated under the DP conditions in the absence of Au precursor (referred to as DP_IM_Pd/TiO_2). Compared to the starting Pd/TiO_2, the Pd particle size decreased and the particle size distribution became more uniform on the DP_IM_Pd/TiO_2. In the presence of Au precursor ($Au/Pd/TiO_2$), Au particles may precipitate on these small Pd particles, forming Au–Pd alloys with Au rich on the surface.

3.2 Catalytic behavior

3.2.1 Hydrogenation of 1-heptyne

The catalytic behavior of the TiO_2 supported Au, Pd, Pd/Au, and Au/Pd catalysts was evaluated in the liquid-phase semihydrogenation of 1-heptyne. The conversion of 1-heptyne and the selectivity to 1-heptene as a function of reaction time are shown in **Figure 10**. The hydrogenation rate was in the order: $Au/Pd/TiO_2$ > Pd/TiO_2 > $Pd/Au/TiO_2$ >> Au/TiO_2. The conversion of 1-heptyne was completed in 30 min and 60 min for the $Au/Pd/TiO_2$ and the $Pd/Au/TiO_2$, respectively under the conditions used. The hydrogenation activity was in accordance with the exposed Pd surface as determined by the CO chemisorption. The very low catalytic activity of the Au/TiO_2 corresponded to the relatively large Au particles being formed. The size of Au particles that was reported to be highly active in hydrogenation reactions usually falls in the range of 2-4 nm [28]. The Au particle size effect, however, varied largely depending on the nature of the substrate molecules. For examples, the reaction with Au/TiO_2 is structure sensitive in the hydrogenation of crotonaldehyde, in which the specific activity of small Au particles (ca. 2 nm) is larger by almost an order of magnitude compared to that of larger Au particles (5-9 nm) [28] whereas it exhibited a structure insensitive characteristic in the 1,3-butadiene hydrogenation [47].

Comparison of the specific activity of supported Au and Pd catalysts in the liquid-phase alkyne hydrogenation has been scarcely reported. Parvulescu et al. [26] reported the catalytic properties of SiO_2-embedded Pd, Au, and Pd–Au alloy colloids with particle sizes in the range of 3-5 nm in the liquid-phase hydrogenation. For the hydrogenation of styrene, the activity of monometallic Pd surpassed those of Pd–Au and Au (Pd > Pd-Au >> Au) whereas in the hydrogenation of cinnamaldehyde and 3-hexyn-1-ol, the catalyst activity was in the order Pd-Au > Pd >> Au. The poor

hydrogenation activity of Au colloids embedded in SiO_2, however, was in line with the results of 1-heptyne hydrogenation over Au/TiO_2 in this study.

All the present catalysts exhibited high selectivity of 1-heptene (> 95%) up to nearly full conversion of 1-heptyne. It is suggested that heptene products were adsorbed more weakly than 1-heptyne on these catalysts. Hence, once formed, heptene molecules were more easily desorbed than the alkyne molecules [48]. Generally, the selectivity of Pd is based on the triple bond being more strongly adsorbed on the active centers than the corresponding double bond, which is due to its high electron density and restricted rotation [49,50]. In the partial hydrogenation of alkyne, a decrease in alkene selectivity usually occurs at close to complete conversion of the alkyne because of the ability of alkene to be re-adsorbed under such conditions [51]. In the liquid-phase hydrogenation of 1-heptyne under mild conditions (reaction temperature 30^oC and H_2 pressure 1.5 bar), the commercial Lindlar catalysts was reported to exhibit 50-85% selectivity to 1-heptene at 47-90% conversion of 1-heptyne [52-54]. Improvement in the catalyst performances has been recently reported over the bimetallic $W\text{-}Pd/\gamma\text{-}Al_2O_3$ (95% 1-heptene selectivity at 100% heptyne conversion) [50] and the Pd/TiO_2 synthesized by one-step flame spray pyrolysis (90% 1-heptene selectivity at 100% heptyne conversion [6]. However, the selectivity trend after complete conversion of 1-heptyne was seldom concerned whilst providing better comparison of the catalyst performances in the alkyne hydrogenation.

During 120 min reaction time, the selectivity of 1-heptene decreased further after complete conversion of 1-heptyne due to the hydrogenation of 1-heptene to heptane. However, the selectivity of 1-heptene still remained > 60% for the $Pd/Au/TiO_2$ and Pd/TiO_2 catalysts whereas it drastically decreased to 0% for the $Au/Pd/TiO_2$. The DP_IM_Pd/TiO_2, which was prepared by treating the Pd/TiO_2 under DP conditions

without Au precursor, exhibited the Pd-like behavior (similar to Pd/TiO_2). It is suggested that in the bimetallic Au–Pd alloy, the Au species should act as an electronic promoter for Pd and greatly promote the second step of hydrogenation of 1-heptene to heptane. The performance plot in terms of selectivity to 1-heptene versus conversion of 1-heptyne is shown in **Figure 11**. It shows that 1-heptene hydrogenation occurred only at nearly complete conversion of 1-heptyne over the catalysts.

3.2.2 Hydrogenation of 1-heptene

The hydrogenation of 1-heptene was carried out in the same manner as that of 1-heptyne hydrogenation under similar conditions. The conversion of 1-heptene as a function of reaction time of the Pd/TiO_2 and the Pd–Au bimetallic catalysts is shown in **Figure 12**. The conversion of 1-heptene at 120 min reaction time was in the order: $Au/Pd/TiO_2$ (100%) > Pd/TiO_2 (46%) > $Pd/Au/TiO_2$ (37%), which was found to be in good agreement with the selectivity of 1-heptene after full conversion of 1-heptyne in 1-heptyne hydrogenation. These results confirm that the hydrogenation of 1-heptene occurred only at nearly or full conversion of 1-heptyne on these catalysts. It has been suggested that the alkyne compound displaces the alkene from the catalyst surface and prevent its re-adsorption, thereby exerting a poisoning effect for the subsequent alkene hydrogenation, which holds as long as the alkyne species is present [54,55] . In other words, the adsorption coefficient of 1-heptyne was greater than that of 1-heptene.

3.2.3 Activity-structure relation

Alkyne hydrogenation has often been regarded as structure insensitive reaction, which is in line with the results in this study. The hydrogenation rate increased with increasing number of exposed Pd surface. The monometallic Pd/TiO_2, $Pd/Au/TiO_2$, and

DP_IM_Pd/TiO_2 exhibited moderately high 1-heptene selectivity after full conversion of 1-heptyne. These catalysts differed in the degree of Pd dispersion (Pd particle size) with the absence of electronic effect. Therefore, it can be summarized that the changes in Pd dispersion (particle size) do not affect the selectivity to 1-heptene in the partial hydrogenation of 1-heptyne. This conclusion follows the well established trend in the literature that the selectivity to alkene formation was irrespective of the Pd particle diameter for most reactants in the selective alkyne hydrogenation [56-58].

The Pd/Au/TiO_2 contained monometallic Pd and bimetallic Pd/Au particles (Fig. 8). It is difficult to estimate the numbers of these monometallic and bimetallic particles. One can say, however, that the size of the latter was large (Fig. 3) and the Au species was absent on the surface of these particles (Table 2). As a result, this Pd/Au/TiO_2 catalyst should have catalytic features similar to the monometallic Pd one in the hydrogenation of either 1-heptyne or 1-heptene. Another Au/Pd/TiO_2 catalyst also contained both monometallic Pd and Pd/Au bimetallic particles. For this catalyst, in contrast to the Pd/Au/TiO_2, the size of bimetallic particles was small (Figs. 4 and 8) and the Au species existed on their surface (Table 2). It can be assumed that there operate electronic interactions between the Pd and Au species in the small bimetallic particles and this modifies the catalytic features of the Pd particles. Again it is difficult to estimate quantitatively the respective contributions of the monometallic and bimetallic particles to the overall catalytic performance. After considering the hydrogenation reaction results obtained with 1-heptyne and 1-hetene, however, it is suggested that the contribution of the bimetallic particles is larger than that of the monometallic ones. This is because its selectivity to 1-heptane was significantly large compared to the other catalysts; the hydrogenation of 1-heptyne to 1-heptene takes place similarly on the surface of monometallic and bimetallic particles while the following hydrogenation of

1-heptene to heptane occurs preferentially on the bimetallic particles. That is, the modification of Pd species by Au was less significant for the first step of hydrogenation of 1-heptyne to 1-heptene than the second step hydrogenation of 1-heptene to heptane. The hydrogenation of 1-heptene on Pd should be more sensitive to the electronic effect than that of 1-heptyne under the reaction conditions used.

The preparation methods chosen in this study were among the most commonly used methods for preparation of supported Pd and Au catalysts. They are very simple and can be reproduced easily; however, they usually contained both monometallic and bimetallic nanoparticles. Simultaneous loading of Pd and Au using non-colloidal route by either IM or DP often led to non-uniform particle size distribution with the presence of fairly large isolated Au particles [59-61]. Improvement in particle size distribution and metal domains distributions of Au-Pd bimetallic catalysts has been achieved using more sophisticated techniques such as sol-immobilization [62] and metal vapor deposition [63]. The present work demonstrated that a combination of IM and DP methods can result in both alloying and non-alloying effects of the bimetallic Au-Pd particles depending on the loading sequence. Nevertheless, all the Au particles appeared to be incorporated with the Pd and there was no separate formation of pure Au nanoparticles in the bimetallic catalyst systems. DP of Au after IM of Pd on the TiO_2 led to more uniform particle size distribution of both monometallic Pd and bimetallic Au-Pd nanoparticles. Although it is difficult to estimate the number of these monometallic and bimetallic particles on the support, their contributions to the overall catalytic performance in the hydrogenation of 1-heptyne and 1-heptene are quite evident. In addition, the exertion of electronic interaction between Pd and Au species, which resulted in modification of catalytic features of the Pd particles, was found only in the smaller bimetallic particles (i.e., < 10 nm). Thus, these results emphasize the

importance of Au-Pd particle size for the electronic interaction to appear and modify the catalytic performance of the Au-Pd bimetallic particles in hydrogenation of 1-heptyne and, probably, in other hydrogenation reactions.

4. Conclusions

The TiO_2 supported Pd/Au catalysts were prepared with the combination of IM and DP methods. DP of Au first followed by IM of Pd ($Pd/Au/TiO_2$) led to large Au aggregates (~30-50 nm) and lower Pd dispersion whereas smaller Pd-Au alloy particles (~4-10 nm) and higher Pd dispersion were obtained when Au was added on the Pd/TiO_2 ($Au/Pd/TiO_2$). Without the electronic modification, the hydrogenation rate increased with increasing number of exposed Pd atoms and there were no significant changes in the 1-heptene selectivity after complete conversion of 1-heptyne. In the presence of alloying effect in the $Au/Pd/TiO_2$, the Au species acted as an electronic promoter for Pd, which greatly promoted the second step hydrogenation of 1-heptene to heptane. As a consequence, the selectivity of 1-heptene decreased drastically to 0%. The heptene hydrogenation was more sensitive to the electronic effect than the hydrogenation of 1-heptyne.

Acknowledgements

We gratefully thank the Dusadeepipat scholarship from Chulalongkorn University, the Thailand Research Fund (TRF), and the Commission on Higher Education for the financial supports of this work. The authors also acknowledge support from the National Research Council of Thailand (NRCT) and Japan Society for the Promotion of Science (JSPS) under the Joint Research Program.

References

1. M. Al-Herz, M.J.H Simmons, J. Wood, Ind. End. Chem. Res. 51 (2012) 8815-8825.
2. M. Crespo-Quesada, R.R. Dykeman, G. Laurenczy, P.J. Dyson, L. Kiwi-Minsker, J. Catal. 279 (2011) 66-74.
3. N. Semagina, A. Renken, L. Kiwi-Minsker, Chem. Eng. Sci. 62 (2007) 5344-5348.
4. D.A. Liprandi, E.A.Cagnola, M.E. Quiroga, P.C. L'Argentiere, Catal. Lett. 128 (2009) 423-433.
5. C.R. Lederhos, P.C. L'Argentiere N.S. Figoli, Ind. Eng. Chem. Res. 44 (2005) 1752-1756.
6. O. Mekasuwandumrong S. Somboonthanakij, P. Praserthdam, J. Panpranot, Ind. Eng. Chem. Res. 48 (2009) 2819-2825.
7. S. Somboonthanakij, O. Mekasuwandumrong, J. Panpranot, T. Nimmanwudtipong, R. Strobel, S.E. Pratsinis, P. Praserthdam, Catal. Lett. 119 (2007) 346-352.
8. A. Papp, A. Molnar, A. Mastalir, Appl. Catal. A 289 (2005) 256-266.
9. P. Weerachawanasak, O. Mekasuwandumrong, M. Arai, S.-I. Fujita, P. Praserthdam, J. Panpranot, J. Catal. 262 (2009) 199-205.
10. J. Panpranot, K. Phandinthong, T. Sirikajorn, M. Arai, P. Praserthdam, J. Mol. Catal. A 261 (2007) 29-35.
11. N. Marin-Astorga, G. Pecchi, J.L.G. Fierro, P. Reyes, J. Mol. Catal. A 231 (2005) 67-74.
12. G. Panzera, V. Modafferi, S. Candamano, A. Donato, F. Frusteri, P.L. Antonucci, J. Power Sources 135 (2004) 177-183.

13. W. Hou, N.A. Dehm, R.W.J. Scott, J. Catal. 253 (2008) 22-27.

14. C. Qi, J. Huang, S. Bao, H. Su, T. Akita, M. Haruta, J. Catal. 281 (2011) 12-20.

15. G. Li, J. Edwards, A.F. Carley, G.J. Hutchings, Catal. Today 122 (2007) 361-364.

16. H.I. Abbott, A. Aumer, Y. Lei, C. Asokan, R. J. Meyer, M. Sterrer, S. Shaikhutdinov, H.-J. Freund, J. Phys. Chem. C 2010, 114, 17099-17104.

17. B. Pawelec, E. Cano-Serrano, J.M. Campos-Martin, R.M. Navarro, S. Thomas, J.L.G. Fierro, Appl. Catal. A, 275 (2004) 127-139.

18. A.M. Venezia, V. La Parola, B. Pawelec, J.L.G. Fierro, Appl. Catal. A, 264 (2004) 43-51.

19. A. Sarkany, O. Geszti, G. Safran, Appl Catal A, 350 (2008) 157-163.

20. A. Sarkany, A. Horvath, Appl. Catal. A 229 (2002) 117-125.

21. A.C. Krauth, G.H. Bernstein, E.E. Wolf, Catal. Lett. 45 (1997) 177-186.

22. M. Harada, K. Asakura, N. Toshima, J. Phys. Chem. 97 (1993) 5103-51 14.

23. X. Yang, D. Chen, S. Liao, H. Song, Y. Li, Z. Fu, Y. Su, J. Catal. 291 (2012) 36-43.

24. R. Liu, Y. Yancun, K. Yoshida, G. Li, H. Jiang, M. Zhang, F. Zhao, S.-I. Fujita, M. Arai, J. Catal. 269 (2010) 191-200.

25. F. Menegazzo, P. Canton, F. Pinna, N. Pernicone, Catal. Commun. 9 (2008) 2353-2356.

26. V.I. Parvulescu, V. Parvulescu, U. Endruschat, G. Filoti, F.E. Wagner, C. Kubel, R. Richards, Chem. Eur. J. 12 (2006) 2343-2357.

27. P. Dash, N.A. Dehm, R.W.J. Scott, J. Mol. Catal. A 286 (2008) 114-119.

28. R. Zanella, C. Louis, S. Giorgio, R. Touroude, J. Catal. 223 (2004) 328-339.

29. S.S. Watson, D. Beydoun, J.A. Scott, R. Anal, Chem. Eng. J. 95 (2003) 213-220.

30. N. Bogdanchikova, A. Pestryakov, M.H. Farias, J.A. Diaz, M. Avalos, J. Navarrete, Solid State Sci. 10 (2008) 908-914.

31. S. Schimpf, M. Lucas, C. Mohr, U. Rodemerck, A. Bruckner, J. Radnik, H. Hofmeister, P. Claus, Catal. Today 72 (2002) 89-94.

32. M. Haruta, N. Yamada, T. Kobayashi, H. Kageyama, B. Delmon, M.J. Genet, J. Catal. 144 (1993) 175-180.

33. G.C. Bond, D.T. Thompson, Catal. Rev. Sci. Eng. 41 (1999) 319-388.

34. A. Herzing, A. F. Carley, J. K. Edwards, G. J. Hutchings, and C. J. Kiely, Chem. Mater. 20 (2008) 1492-1501.

35. D.I. Enache, J.K. Edwards, P. Landon, B. Solsona-Espriu, A.F. Carley, A.A. Herzing, M. Watanabe, C.J. Kiely, D.W. Knight, G.J. Hutchings, Science 311 (2006) 362-365.

36. R. Zanella, L. Delannoy, C. Louis, Appl. Catal. A 291 (2005) 62-72.

37. S. Ivanova , V. Pitchon, C. Petit, H. Herschbach, A. V. Dorsselaer, E. Leize, Appl. Catal. A 298 (2006) 203-210.

38. J. Pollmann, R. Franke, J. Hormes, H. Bonnemann, W. Brijoux, A. S. Tilling, J. Elec. Spec. Rel. Phen. 94 (1998) 219-227.

39. A.M. Venezia, V. La Parola, V. Nicoli, G. Deganello, J. Catal. 212 (2002) 56-62.

40. A.M. Venezia, V. La Parola, G. Deganello, B. Pawelec, J.L.G. Fierro, J. Catal. 215 (2003) 317-325.

41. K. Qian, W. Huang, Catal. Today 164 (2011) 320-324.

42. X. Yang, D. Chen, S. Liao, H. Song, Y. Li, Z. Fu, Y. Su, J. Catal. 291 (2012) 36-43.

43. J. Huang, W.-L. Dai, H. Li, K. Fan, J. Catal. 252 (2007) 69-76.

44. J.A. Creighton, D.G. Eadon, J. Chem. Soc. Faraday Trans. 87 (1991) 3881-3891.

45. R.W.J. Scott, O.M. Wilson, S.-K. Oh, E.A. Kenik, R.M. Crooks, J. Am. Chem. Soc.126 (2004) 15583-15591.

46. P. Dash, N.A. Dehm, R.W.J. Scott, J. Mol. Catal. A 286 (2008) 114-119.

47. M. Okumura, T. Akita, M. Haruta, Catal. Today 74 (2002) 265-269.

48. T. A. Nijhuis, G. van Koten, J.A. Moulijn, Appl. Catal. A 238 (2003) 259-271.

49. A. Molnar, A. Sarkany, M. Varga, J. Mol. Catal. A 173 (2001) 185-221.

50. H. Molero, B.F. Bartlett, W.T. Tysoe, J. Catal. 181 (1999) 49-56.

51. G.C.Bond, Metal-catalysed reactions of hydrocarbons, Springer, New York, 2005.

52. R. Lederhos, M. J. Maccarrone, J. M. Badano, G. Torres, F. Coloma-Pascual, J. C. Yori, M. E. Quiroga, Appl. Catal. A 396 (2011) 170-176.

53. C.R. Lederhos, J. M. Badano, M. E. Quiroga, P. C. L'Argentière, Quim. Nova 33 (2010) 816-820.

54. P.C. L'Argentiere, E. A. Cagnola, M. E. Quiroga, D. A. Liprandi, Appl. Catal. A 226 (2002) 253-263.

55. M. Varga, A. Molnar, M. Mohai, I. Bertoti, M. Janik-Czachor, A. Szummer, Appl. Catal. A 234 (2002) 167-178.

56. A. Sarkany, A. Beck, A. Horvth, Zs. Revay, L. Guczi, Appl. Catal. A 253 (2003) 283-292.

57. J.G. Ulan, W.F. Maier, D.A. Smith, J. Org. Chem. 52 (1987) 3132-3142.

58. P. Albers, K. Seibold, G. Prescher, H. Muller, Appl. Catal. A 176 (1999) 135-146.

59. P. J. Miedziak, Q. Heb, J. K. Edwards, S. H. Taylor, D. W. Knight, B. Tarbit, C. J. Kielyb, G.J. Hutchings, Catal. Today 163 (2011) 47–54.

60. S. Hermans, A. Deffernez, M. Devillers, Appl. Catal. A 395 (2011) 19–27.

61. J. K. Edwards, J. Pritchard, M. Piccinini, G. Shaw, Q. He, A. F. Carley, C.J. Kiely, G.J. Hutchings, J. Catal. 292 (2012) 227–238.

62. J.A. Lopez-Sanchez, N. Dimitratos, N. Glanville, L. Kesavan, C. Hammond, J.K. Edwards, A.F. Carley, C.J. Kiely, G.J. Hutchings, Appl. Catal. A 391 (2011) 400–406.

63. C. Evangelisti, E. Schiavi, L.A. Aronica, A.M. Caporusso, G. Vitulli, L. Bertinetti, G. Martra, A. Balerna, S. Mobilio, J. Catal. 286 (2012) 224–236.

Table 1 Loading sequence in the catalyst preparation

Catalyst	First step		Second step	
	Metal	Method	Metal	Method
Au/TiO_2	Au	DP	−	−
Pd/TiO_2	Pd	IM	−	−
$Pd/Au/TiO_2$	Au	DP	Pd	IM
$Au/Pd/TiO_2$	Pd	IM	Au	DP

Metal loading: Au 1 wt%, Pd 0.5 wt%.

DP: Deposition-precipitation, IM: Incipient wetness impregnation.

Table 2 Characteristics of various TiO_2 supported Pd, Pd/Au, and Au/Pd catalysts [a]

Sample	CO Chemisorption		Pd $3d_{5/2}$		Au $4f_{7/2}$		Atomic concentration [b]	
	%D	d_p Pd^0 (nm)	B.E. (eV)	FWHM (eV)	B.E. (eV)	FWHM (eV)	Pd (%)	Au (%)
Au/TiO_2	n/a	n/a	n/a	n/a	83.0	1.176	n/a	0.08
Pd/TiO_2	13.4	8.4	336.5	1.844	n/a	n/a	0.28	n/a
$Pd/Au/TiO_2$	6.8	16.4	336.8	2.794	n.d.	1.352	0.70	n.d.
$Au/Pd/TiO_2$	27.6	4.0	(1) 335.2 (2) 336.2	1.161 1.611	83.1	1.287	(1) 0.91 (2) 0.17	0.67

a. %D: Degree of Pd dispersion, d_p: Average diameter of Pd particles, B.E.; Binding energy, FWHM: Full width at half maximum.
b. From XPS.

Figure Captions

Figure 1 XRD patterns of Au/TiO_2, Pd/TiO_2, $Pd/Au/TiO_2$, and $Au/Pd/TiO_2$.

Figure 2 TEM images and particle size distribution of TiO_2 supported Au and Pd catalysts.

Figure 3 TEM images of $Pd/Au/TiO_2$.

Figure 4 TEM images of $Au/Pd/TiO_2$.

Figure 5 XPS Pd 3d core level spectra of Pd/TiO_2, $Pd/Au/TiO_2$, and $Au/Pd/TiO_2$.

Figure 6 XPS Au 4f core level spectra of Au/TiO_2, $Pd/Au/TiO_2$, and $Au/Pd/TiO_2$.

Figure 7 UV-vis spectra of Au/TiO_2, Pd/TiO_2, $Pd/Au/TiO_2$, and $Au/Pd/TiO_2$.

Figure 8 A schematic drawing illustrating the catalyst morphology

Figure 9 TEM images of DP_IM_Pd/TiO_2 catalyst.

Figure 10 Hydrogenation of 1-heptyne on Pd/TiO_2, $Pd/Au/TiO_2$, and $Au/Pd/TiO_2$: %heptyne conversion (a) and %1-heptene selectivity (b).

Figure 11 The performance plots of 1-heptyne hydrogenation over the various catalysts

Figure 12 Hydrogenation of 1-heptene on Au/TiO_2, Pd/TiO_2, $Pd/Au/TiO_2$, and $Au/Pd/TiO_2$

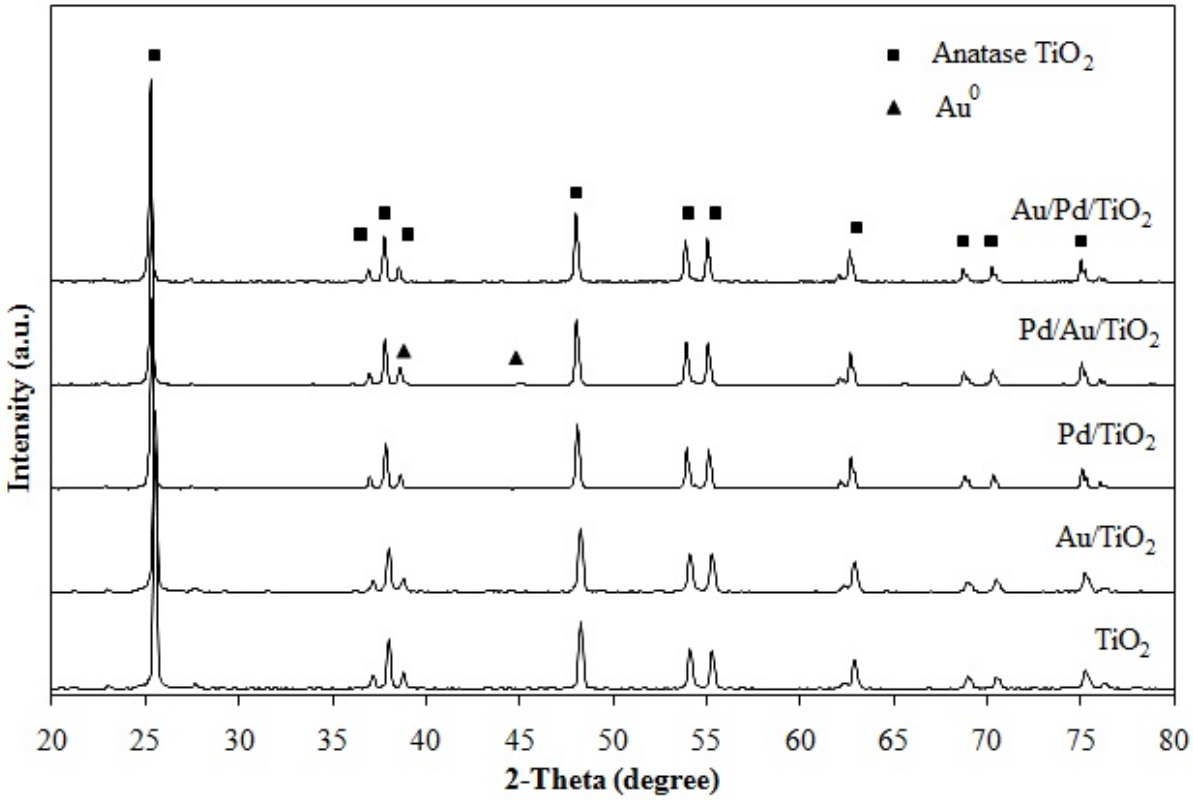
Anatase TiO2
Au0
Au/Pd/TiO2
Pd/Au/TiO2
Pd/TiO2
Au/TiO2
TiO2
Intensity (a.u.)
20
25
30
35
40
45
50
55
60
65
70
75
80
2-Theta (degree)

Figure 1

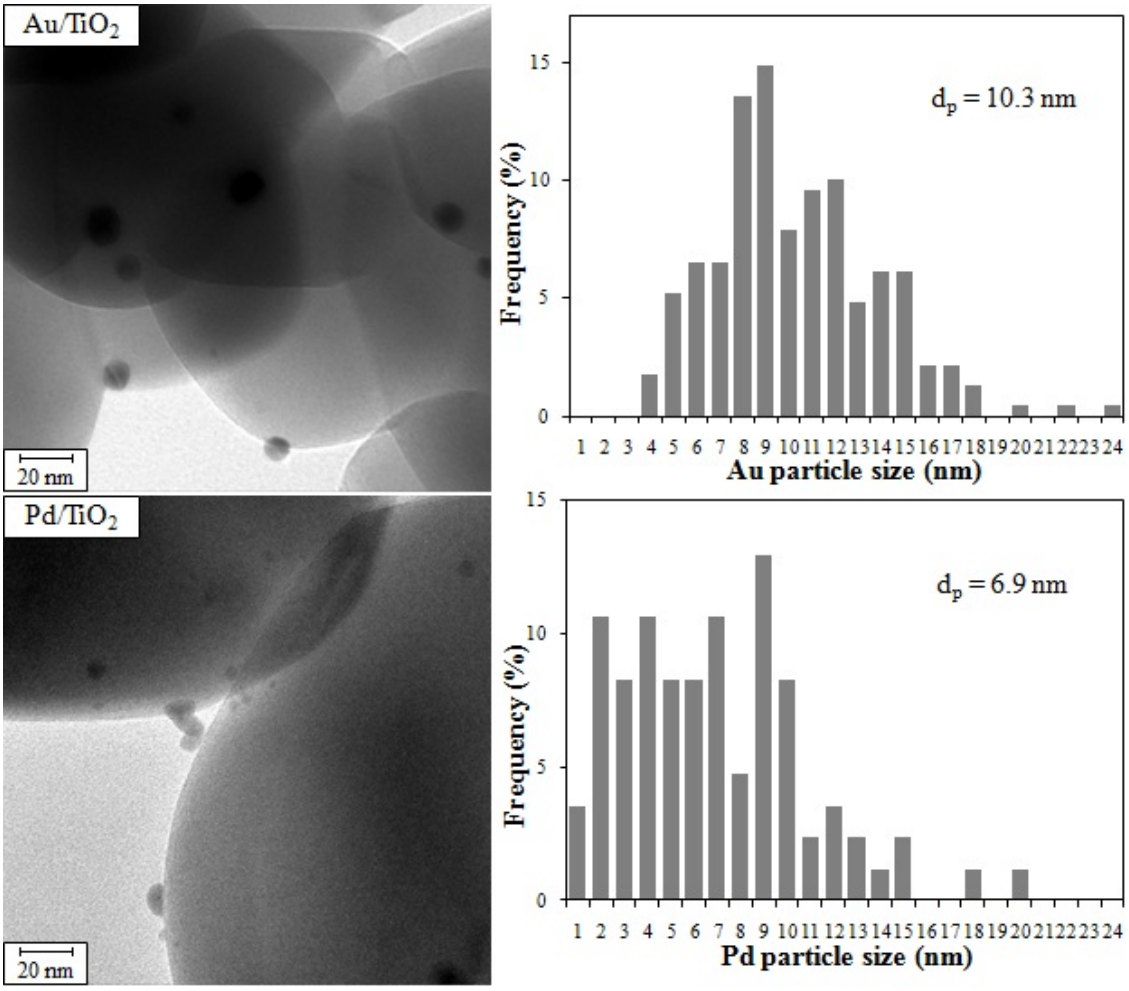
Au/TiO2
20 nm
Pd/TiO2
20 nm
Frequency (%)
dp = 10.3 nm
Au particle size (nm)
dp = 6.9 nm
Pd particle size (nm)

Figure 2

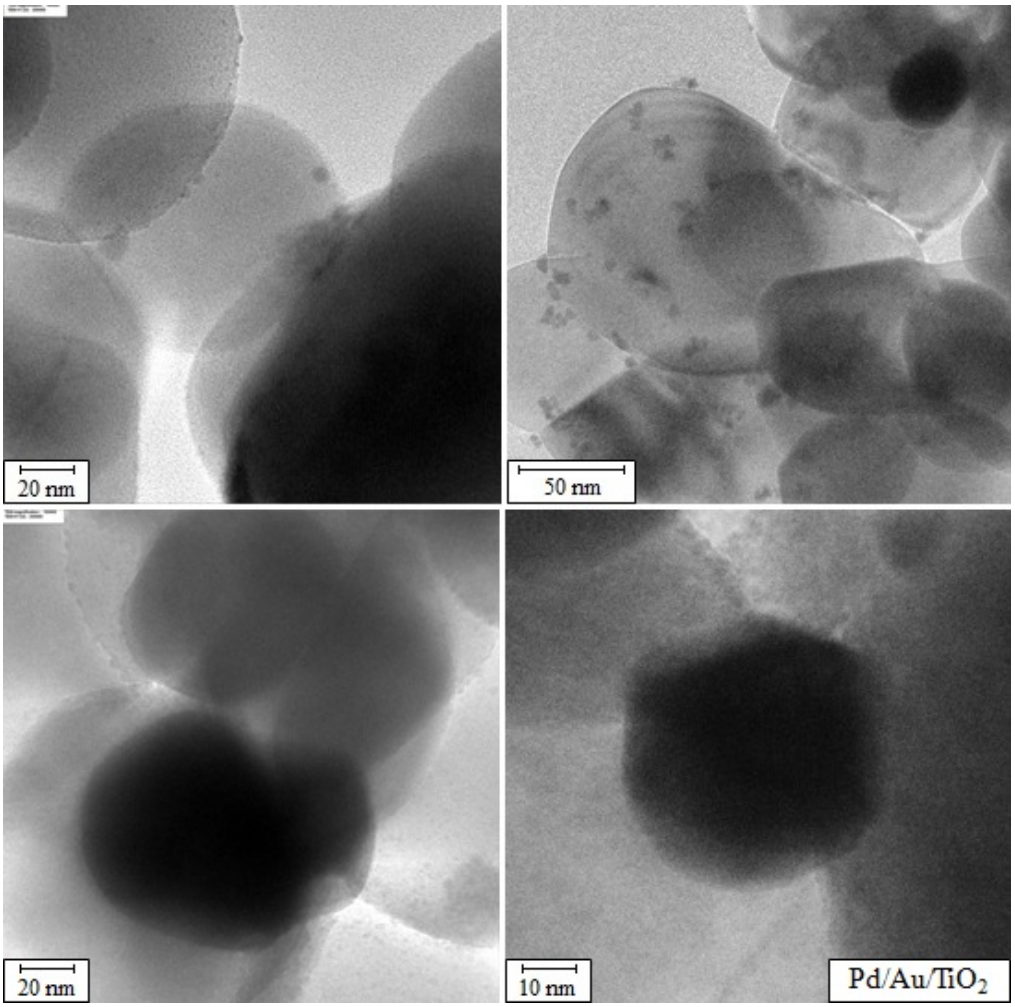

Figure 3

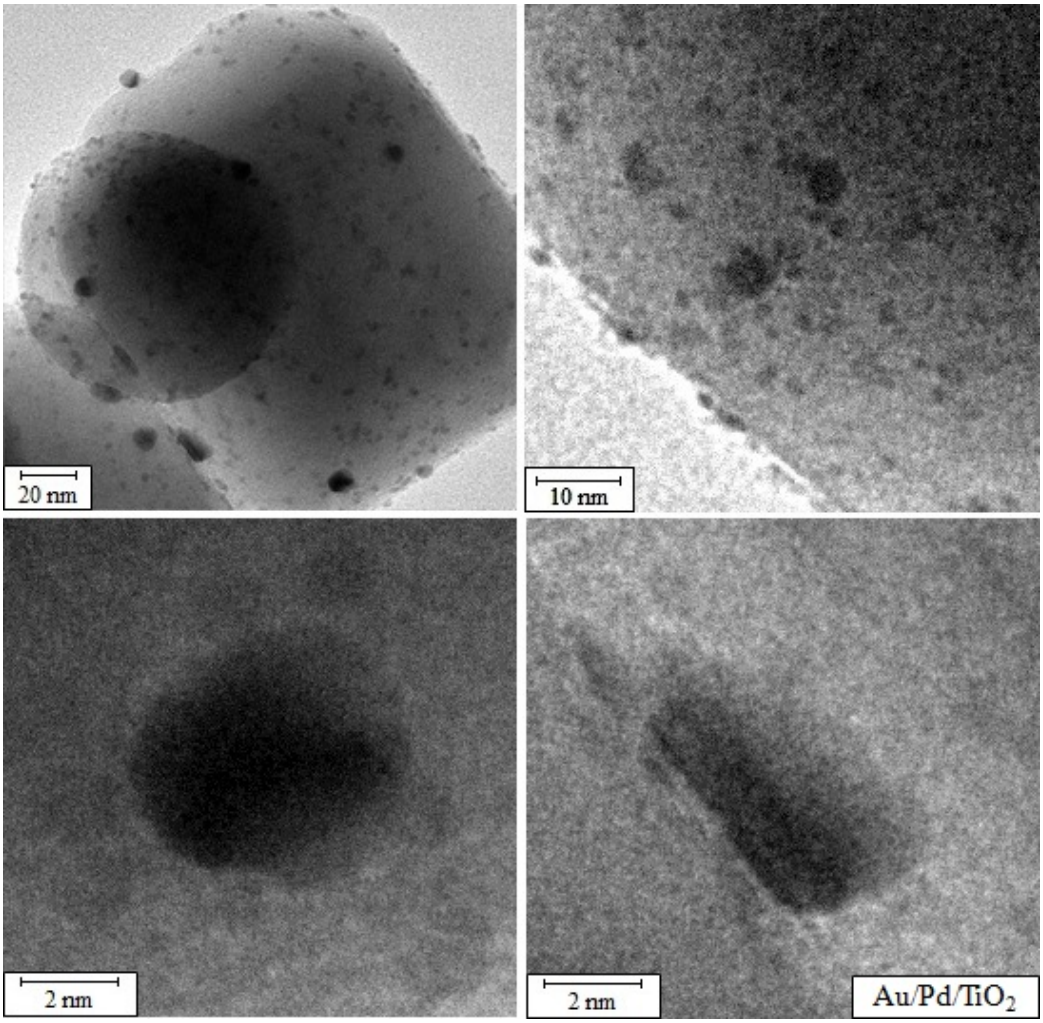

Figure 4

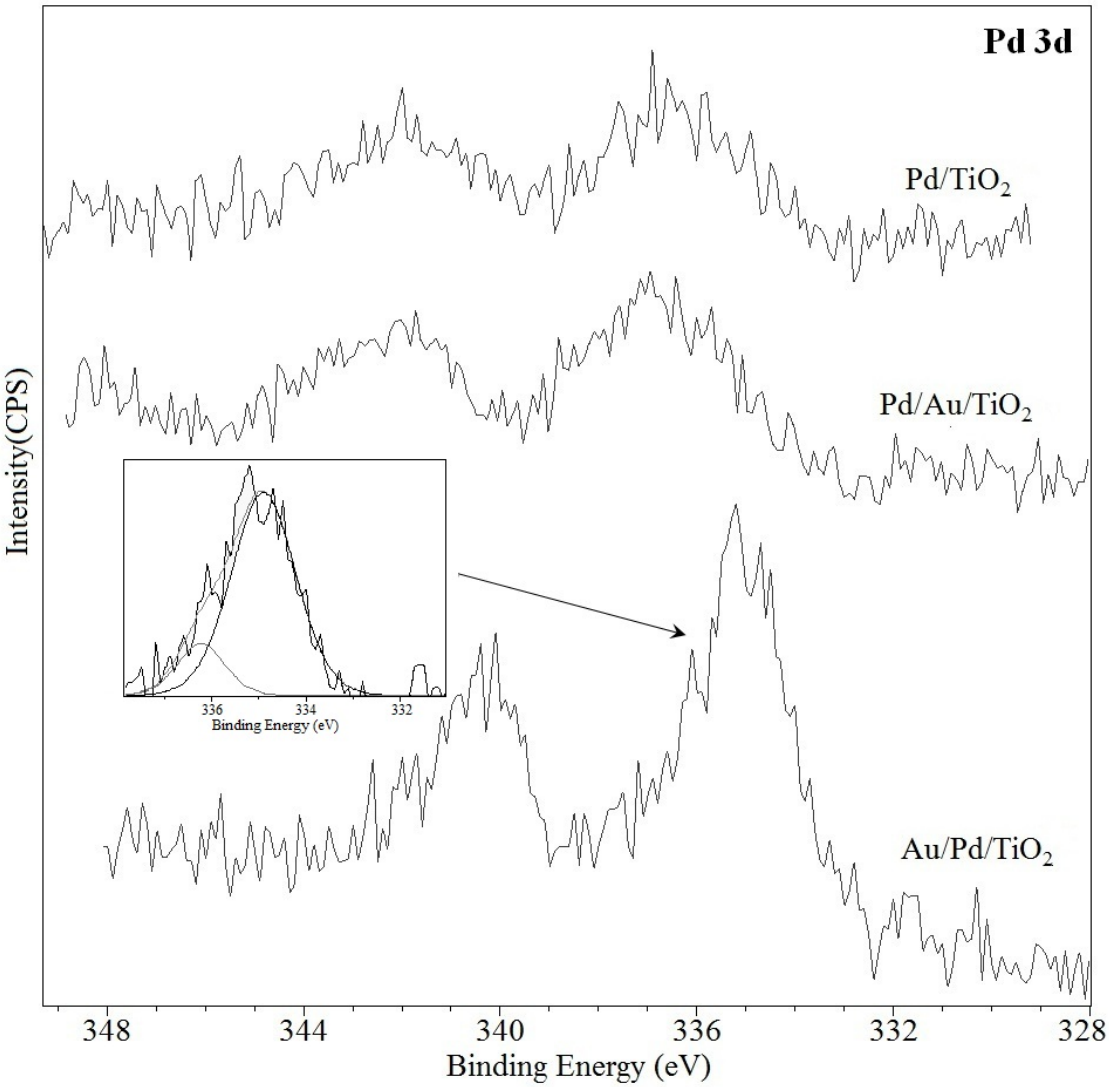
Pd 3d
Pd/TiO2
Pd/Au/TiO2
Au/Pd/TiO2
Intensity(CPS)
336
334
332
Binding Energy (eV)
348
344
340
336
332
328
Binding Energy (eV)

Figure 5

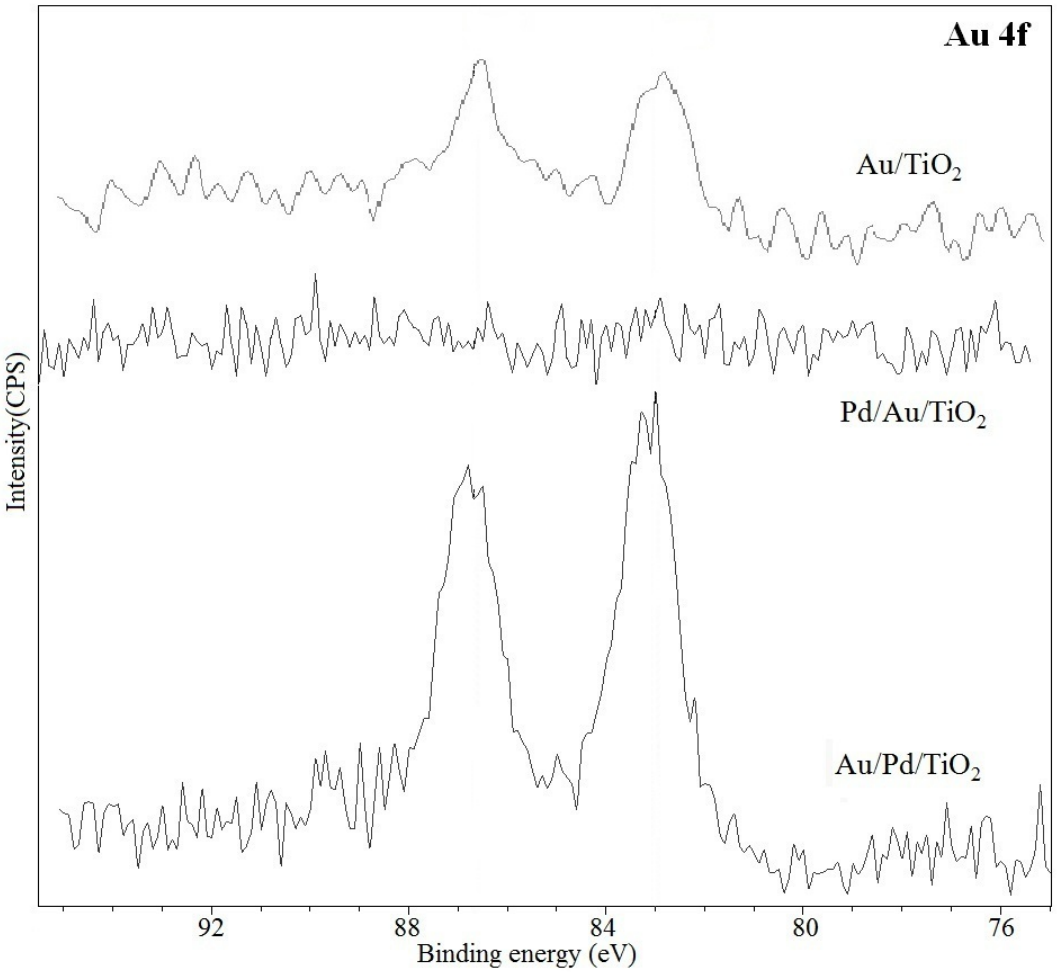
Au 4f
Au/TiO2
Pd/Au/TiO2
Au/Pd/TiO2
Intensity(CPS)
92
88
84
80
76
Binding energy (eV)

Figure 6

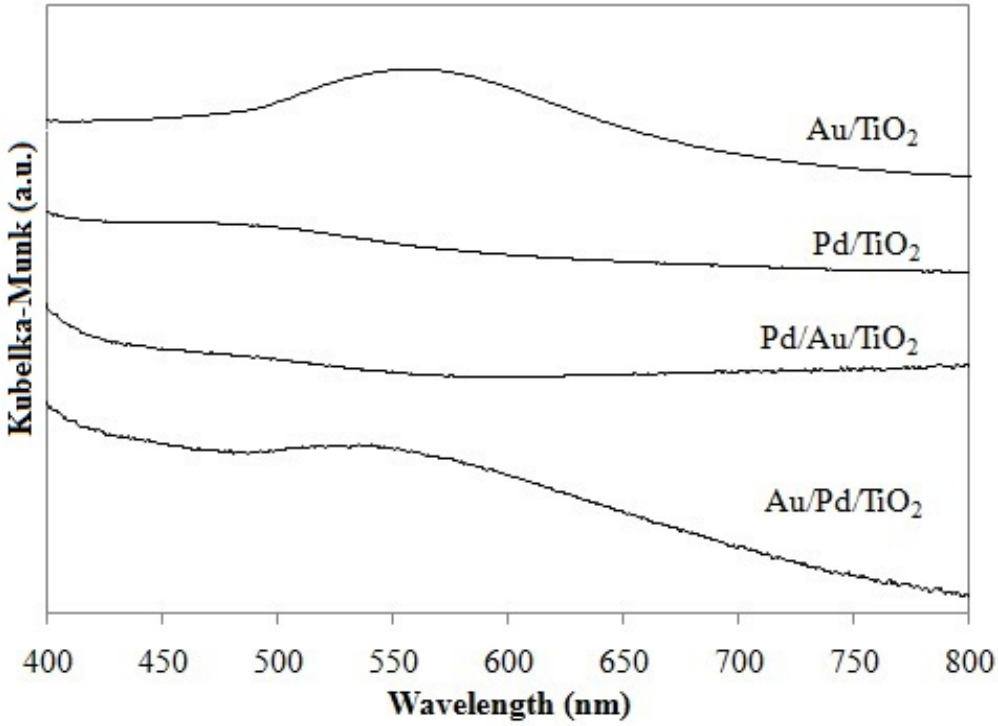
Au/TiO2
Pd/TiO2
Pd/Au/TiO2
Au/Pd/TiO2
Kubelka-Munk (a.u.)
400
450
500
550
600
650
700
750
800
Wavelength (nm)

Figure 7

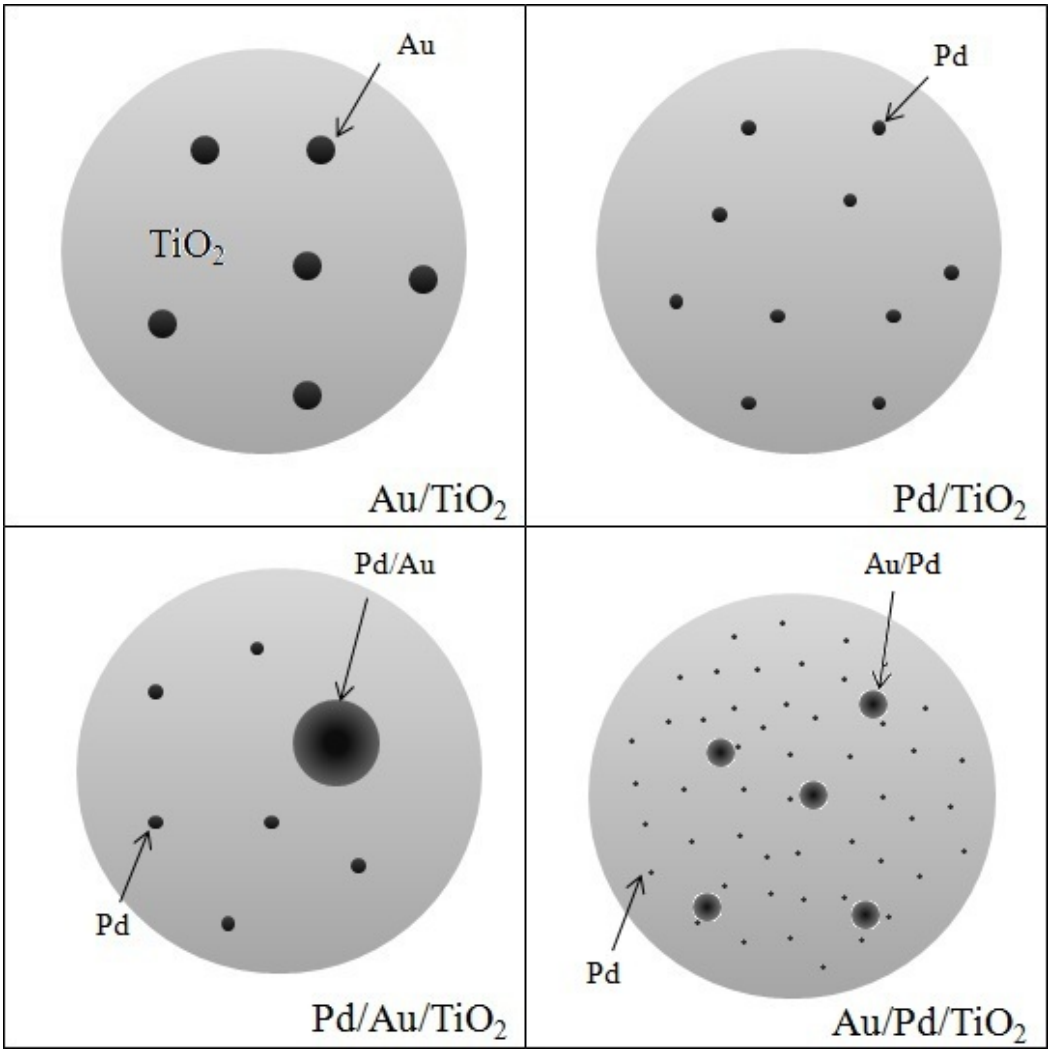

Figure 8

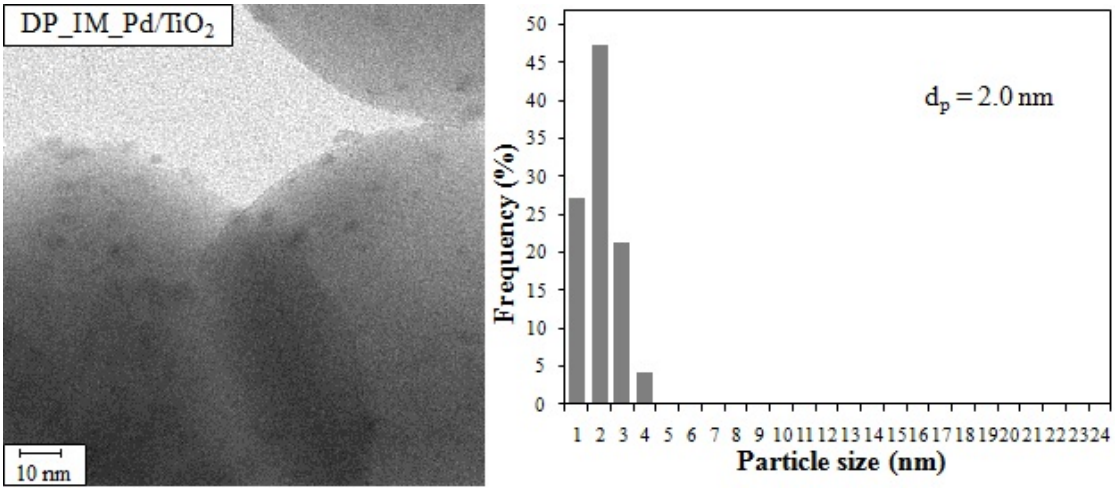

Figure 9

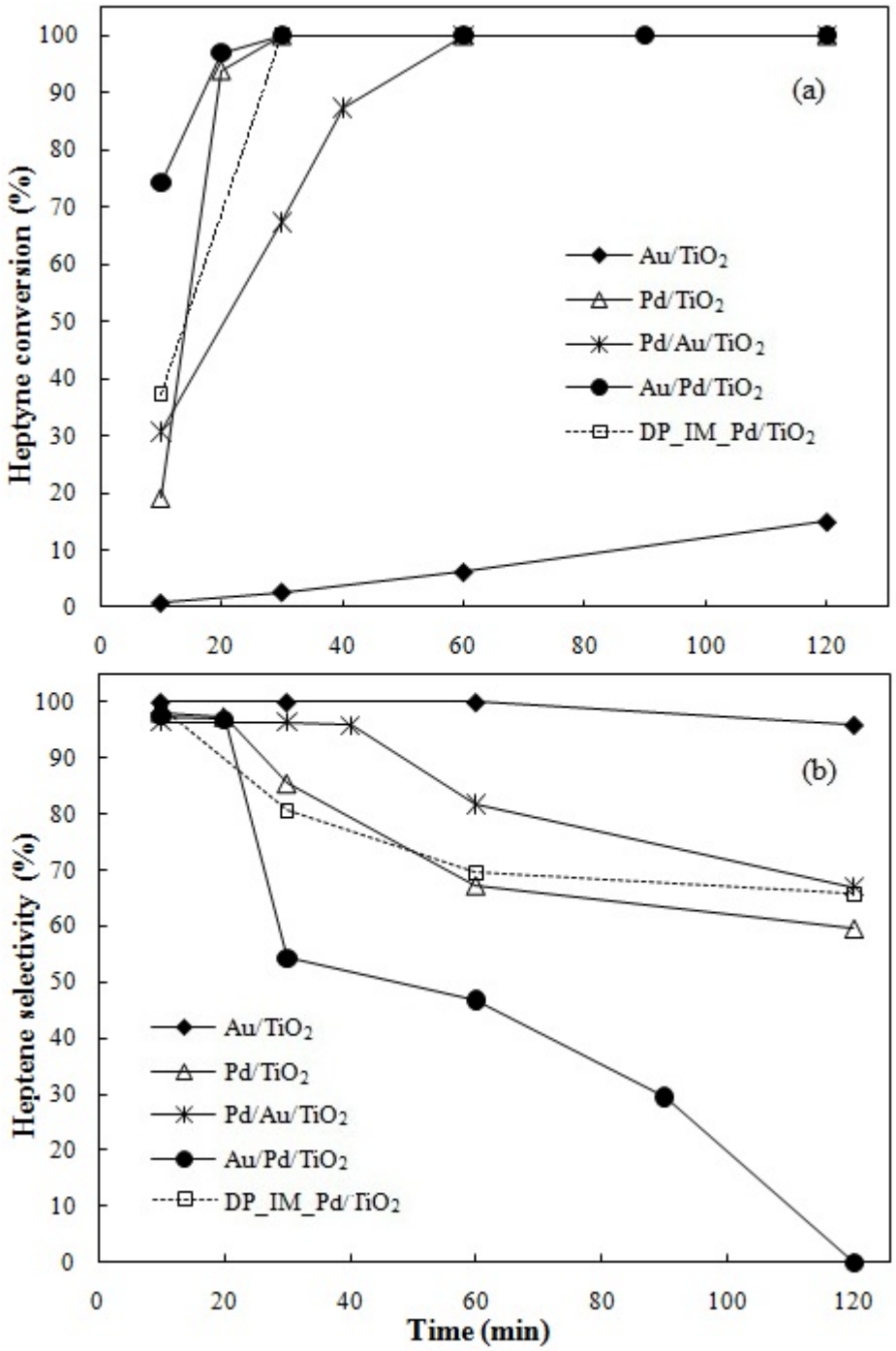
(a)
Heptyne conversion (%)
Au/TiO2
Pd/TiO2
Pd/Au/TiO2
Au/Pd/TiO2
DP_IM_Pd/TiO2
(b)
Heptene selectivity (%)
Time (min)

Figure 10

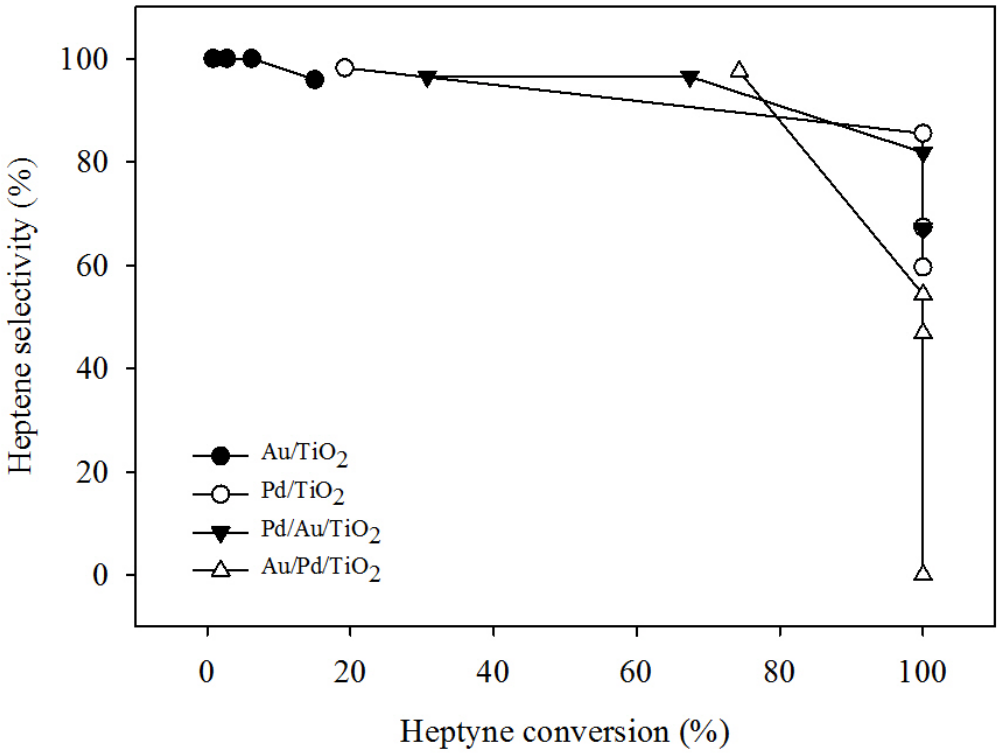
Heptene selectivity (%)
100
80
60
40
20
0
0
20
40
60
80
100
Heptyne conversion (%)
Au/TiO2
Pd/TiO2
Pd/Au/TiO2
Au/Pd/TiO2

Figure 11

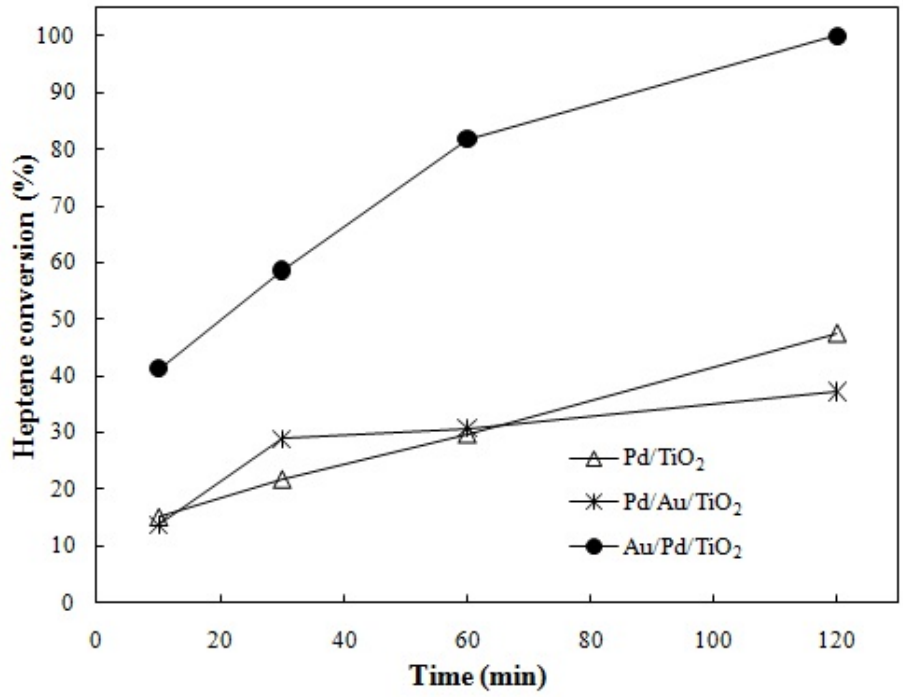
Heptene conversion (%)
Time (min)
Pd/TiO2
Pd/Au/TiO2
Au/Pd/TiO2
0
10
20
30
40
50
60
70
80
90
100
0
20
40
60
80
100
120

Figure 12
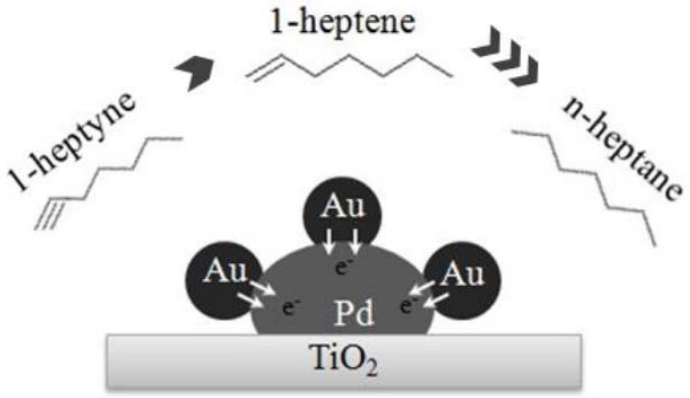
Graphical Abstract